JAIC
Journal of Applied Instrumentation and Control

Frequency Response Comparison of PI-Based and Cascade-Free MPC Field Oriented Control Using 1 kHz SVM Applied to a PMSM Drive

Comparação da Resposta em Frequência do Controlador Orientado a Campo Baseado em PI e em MPC Multivariável Usando SVM de 1 kHz Aplicado a um PMSM

Gabriel H. Negri, Arthur G. Bartsch, Mariana S. M. Cavalca and Ademir Nied

***Abstract* — This paper presents a 1 kHz SVM-FOC (Space Vector Modulation with Field Oriented Control) drive system for a PMSM (Permanent Magnet Synchronous Motor), using different control strategies. Such strategies are internal model and frequency response designed PI (Proportional-Integral) controllers and a multivariable MPC (Model Predictive Control) controller using a state-space prediction model. This MPC method becomes interesting for improving the closed-loop speed frequency response, since it results in a cascade-free controller. The performance of each controller was evaluated in a qualitative manner through reference tracking simulations and quantitatively by load torque and speed reference AC sweeps, generating dynamic stiffness curves and Bode diagrams. Results show that the MPC approach is useful for enabling fast dynamic responses with the reduced switching frequency, which reduces the drive system cost and improves its efficiency.**

***Index Terms*— MPC, FOC, PMSM, Multivariable Control, Frequency Response.**

G.H. Negri is a student for Ph.D. degree at Santa Catarina State University, Joinville, Brazil (e-mail:negri.gabriel@gmail.com).

A. G. Bartsch is an assistant professor at professor at Federal Institute of Santa Catarina, and a student for Ph.D. degree at Santa Catarina State University (email: arthurbartsch@gmail.com).

M. S. M. Cavalca is currently the Graduate Electrical Engineering Program Coordinator at Santa Catarina State University, Joinville, Brazil (email: mariana.cavalca@udesc.br).

A. Nied is an Associate Professor in the Department of Electrical Engineering, Santa Catarina State University, Brazil (email: ademir.nied@udesc.br).

***Resumo* — Este artigo apresenta um sistema de acionamento para um motor síncrono de ímãs permanentes (PMSM) com Controle por Orientação de Campo e Modulação por Vetores Espaciais (SVM-FOC) de 1 kHz usando diferentes estratégias de controle. Tais estratégias são controle Proporcional-Integral (PI) de modelo interno projetado através da resposta em frequência e um Controlador Preditivo (MPC) multivariável com modelo de predição no espaço de estado. Tal método de MPC é útil para melhorar a resposta em frequência da velocidade do motor em malha fechada, pois resulta em um controlador sem cascateamento. O desempenho de cada controlador foi avaliado de forma qualitativa através de simulações de rastreamento de referência e de forma quantitativa por varreduras AC de torque de carga e referência de velocidade, gerando curvas de rigidez dinâmica e diagramas de Bode. Os resultados mostram que a abordagem com MPC é útil para possibilitar respostas dinâmicas rápidas com frequência de chaveamento reduzida, o que pode reduzir o custo do sistema de acionamento e aumentar sua eficiência.**

***Palavras-chave*—MPC, FOC, PMSM, Controle Multivariável, Resposta em Frequência.**

I. Introduction

Permanent Magnet Synchronous Motors (PMSMs) are a class of AC motors which have the main advantages of high power density, high efficiency and low maintenance cost. However, the use of permanent magnets as passive magnetic flux sources generates a higher production cost in relation to

other AC motors, such as three-phase induction motors [1].

The drive system for a three-phase PMSM is usually implemented with a three-phase bridge inverter, controlled by Pulse Width Modulation (PWM) or Space Vector Modulation (SVM). One of the most common forms of driving a three phase PMSM with high efficiency is by using Field Oriented Control (FOC), which is based on transforming the measured AC currents into two phase DC currents by means of Park's transform [2]. With Park's Transform, the currents are decomposed into direct axis (i_d) and quadrature axis currents (i_q). The former is mainly responsible for machine magnetic flux and the latter is mainly related to machine electric torque.

Thus, the FOC scheme is applied to control the machine torque and flux. For a surface-mounted PMSM it is sufficient to establish a null reference to i_d current to accomplish the maximum torque per Ampère (MTPA) condition. Therefore, FOC is composed by an independent i_d regulator and a cascaded speed and torque control loop. The external speed loop is used to achieve null steady-state error for speed reference tracking and disturbance rejection, generating the reference signal for i_q current. This current is controlled in the internal loop, providing the torque to accelerate the machine and to reject load disturbances. Usually, a Proportional-Integral (PI) controller is employed in each loop. The main advantage of using such methodology is the implementation simplicity of PI controllers and low computational cost. However, cascade control design may be limited in frequency, since the current controllers are limited by the switching frequency and the speed controller is usually designed with a 5-10 times smaller bandwidth than current controller to avoid coupling effects.

One possible solution for improving the speed frequency response in a FOC structure is the use of multivariable control methods. An interesting class of multivariable controllers is Model Predictive Control (MPC). More specifically, in this work, a state space motor model was employed within MPC [3]. The advantages of such technique involve consideration of coupled dynamics, which allows the use of a higher bandwidth in the speed controller design. Thus, for a desired speed bandwidth, it is possible to reduce the switching frequency, comparing to a conventional cascaded PI approach, reducing switching losses. Typically, MPC approaches for motor drives are divided into Finite Control Set (FCS) [4], in which the control actions are switching sequences, directly controlling the inverter switches, and Continuous (or Convex) Control Set (CCS) [4, 5] in which the control actions are represented by continuous values and a modulation technique is used to drive the inverter switches. In this work, a CCS-MPC approach was chosen due to the reduced current total harmonic distortion (THD) caused by this control strategy if compared to FCS-MPC. This low THD occurs since CCS-MPC can be combined with SVM, with a fixed switching frequency. This low current THD reduces the torque ripple and vibrations. Also, CCS-MPC usually presents a lower computational burden than FCS (in unconstrained case, with a high prediction horizon), and can be implemented in the same device as the digital PI, as presented in [5, 6].

The objective of this work is to evaluate both PI and MPC methods for FOC by observing tracking of constant references, frequency responses to sinusoidal references and the dynamic stiffness [7] to the application of load torques. As the MPC approach implements FOC in a multivariable loop (cascade-free controller [8, 9]), it is not necessary to consider the cascade effects, which enables a higher bandwidth for the speed controller. Thus, this approach is useful for implementing a FOC algorithm with a limited switching frequency, since the speed controller does not need to be designed with a frequency margin from the current controller.

A contribution of this work is to present the advantages of using a multivariable MPC strategy in relation to conventional cascaded PI controllers, using a frequency domain analysis. Also, the application of proper frequency domain performance metrics is presented with a didactic approach.

This paper is divided as follows. The motor model is explained in Section II. Section III presents the PI controllers design procedure, while the MPC controller is presented in Section IV. Simulation results are shown in Section V. Concluding remarks are given in Section VI.

II. PMSM Model

By means of Park's transform in the rotor reference frame, the model for a surface-mounted PMSM may be given in a state-space form as follows, using $L_e = L - L_m$:

$$\begin{bmatrix} \dot{i_d} \\ \dot{i_q} \\ \dot{\omega_m} \end{bmatrix} = \underbrace{\begin{bmatrix} \frac{-R}{L_e} & -\omega_r & -k_e \\ \omega_r & \frac{-R}{L_e} & 0 \\ 0 & \frac{1.5k_e}{J} & \frac{-B_m}{J} \end{bmatrix}}_{A_c} \begin{bmatrix} i_d \\ i_q \\ \omega_m \end{bmatrix} + \underbrace{\begin{bmatrix} 1/L_e & 0 \\ 0 & 1/L_e \\ 0 & 0 \end{bmatrix}}_{B_c} \begin{bmatrix} v_d \\ v_q \end{bmatrix} \quad (1)$$

$$\omega_r = \frac{P}{2}\omega_m \quad (2)$$

in which ω_m is the rotor mechanical speed, ω_r is the rotor electrical speed, P is the number of poles, B_m is a viscous friction coefficient, J is the rotating parts total inertia, R is the stator phase resistance, L is the stator phase inductance, L_m is the stator mutual inductance, v_d is the stator d-axis input voltage, v_q is the stator q-axis input voltage and k_e is the PMSM torque and back-EMF coefficient. The electromagnetic torque, calculated with dq variables for a surface mounted sinusoidal PMSM with no salient poles, is given by:

$$T_e = 1.5 k_e i_q \quad (3)$$

Using θ_e as the rotor electrical position, Park's transform is applied for a generic set of variables F by [10]:

$$F_{dq} = \frac{2}{3}\begin{bmatrix} \sin(\theta_e) & \sin(\theta_e - \frac{2\pi}{3}) & \sin(\theta_e + \frac{2\pi}{3}) \\ \cos(\theta_e) & \cos(\theta_e - \frac{2\pi}{3}) & \cos(\theta_e + \frac{2\pi}{3}) \end{bmatrix} F_{abc} \quad (4)$$

where $F_{dq} = [f_d \quad f_q]^T$ and $F_{abc} = [f_a \quad f_b \quad f_c]^T$. The utilized motor parameters are presented in Table I.

TABLE I
PMSM PARAMETERS

Parameter	Value	Unit
R	15.5	Ω
L	$76m$	H
L_m	$38m$	H
J	0.1566	Kg m²
B_m	$0.98m$	N m s rad^{-1}
P	48 (24 pairs)	-
k_e	5.6	N m A^{-1}
T_L	20	N m

*m stands for milli and m for meter.

III. PI CONTROLLERS DESIGN

A block diagram for FOC using PI controllers is shown in Figure 1. The speed controller, PI_ω, generates the reference for i_q. The output of PI_{i_q} is the q-axis voltage, v_q. These two controllers compose the cascaded control loop in a PI-based FOC. A third controller, PI_{i_d}, is used to track the reference for i_d, producing the direct axis voltage v_d. To achieve a MTPA condition, the reference for i_d is set to zero. The SVM block is used to perform modulation, driving a three-phase bridge inverter, producing three-phase switched voltage inputs for the PMSM. Rotor electrical position, θ_e, is provided to the SVM block. Feedback for the current control loops is provided through Park's transform.

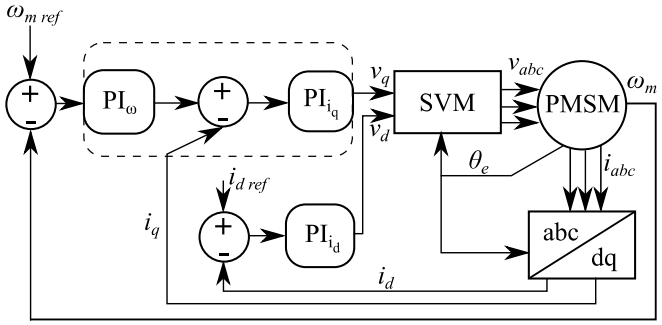

Fig. 1. FOC using PI controllers. The area delimited by the dashed rectangle indicates the use of cascaded control.

The design of the tested PI controllers was performed with the aid of Internal Model Control (IMC) methodology, which consists in combining the inverse model of the plant, a filter and a reference model. By designing the IMC control structure, it is possible to obtain an equivalent conventional controller. For a stable and minimum-phase plant model, it is possible to design a controller such that the closed-loop transfer function is equal to the employed filter transfer function. Such design procedure is given as follows [11]:

- Define a representative transfer function model for the plant, given by $G_c(s)$;
- Specify the closed-loop bandwidth ω_c;
- Design a filter $f(s) = \frac{1}{\left(\frac{s}{\omega_c}+1\right)^n}$, with n equal to the plant order;
- Make $q(s) = \frac{f(s)}{G_c(s)}$,
- Obtain the controller $c(s) = \frac{q(s)}{1-G_c(s)q(s)}$;
- Obtain an equivalent discretized controller for digital implementation.

If the plant is represented by a first order model, this procedure leads to a PI controller:

$$c(s) = K_p + \frac{K_i}{s} \tag{5}$$

The transfer function models for ω_m, i_q and i_d, as functions of i_q, v_q and v_d, respectively, are given below, neglecting the coupling between variables and nonlinearities given by the state space model in (1):

$$\frac{\omega_m(s)}{i_q(s)} = \frac{1.5k_e}{sJ + B_m} \tag{6}$$

$$\frac{i_q(s)}{v_q(s)} = \frac{i_d(s)}{v_d(s)} = \frac{1}{sL_e + R} \tag{7}$$

With this methodology, the obtained controller transfer functions $c_\omega(s)$ and $c_i(s)$ for speed and current, respectively, are:

$$c_\omega(s) = \omega_{c\omega}\frac{sJ + B_m}{1.5k_e s} \tag{8}$$

$$c_i(s) = \omega_{ci}\frac{sL_e + R}{s} \tag{9}$$

Using a switching frequency of 1 kHz, the current bandwidth ω_{ci} was set to 628 rad/s, or 100 Hz. The speed loop bandwidth $\omega_{c\omega}$ was set to 62.8 rad/s, or 10 Hz, to ensure a reasonable decoupling between the controllers.

Regarding the speed controller, using the controller zero $\omega_z = B_m/J$ to cancel the speed pole leads to a very small integrative gain, $K_i = \omega_{c\omega}B_m/(1.5k_e)$. Without any load, this condition does not cause convergence problems. However, when a load torque is applied to motor axis, the closed-loop settling time becomes very high. Due to this, the frequency of the speed controllers zero, ω_z, was set at higher frequencies than the speed pole. Using higher values than $\omega_z = 6000B_m/J$ resulted in highly oscillatory responses, while values smaller than $\omega_z = 300B_m/J$ resulted in slow convergence for motor speed.

Two different tunings for the speed PI and the current loop PI tuning are shown in Table II. We refer to PI-1 as the controllers set composed by PI-1_ω and PI_i (the same tuning is used for i_q and i_d) and PI-2 as the controllers set composed by PI-2_ω and PI_i (the same current loop, PI_i, was used with both PI-1_ω and PI-2_ω).

TABLE II
SPEED AND CURRENT LOOP PI CONTROLLERS' PARAMETERS

	ω_z	K_p	K_i	ω_c
PI-1$_\omega$	$6000B_m/J$	1.171	43.973	62.8 rad/s (10 Hz)
PI-2$_\omega$	$300B_m/J$	1.171	2.198	62.8 rad/s (10 Hz)
PI$_i$	R/L_e	23.88	9734	628 rad/s (100 Hz)

A test of reference tracking and step load rejection was performed for each PI controller set. Figure 2 shows the results for PI-1 while Figure 3 shows the results for PI-2. As it can be observed, in both cases the controllers were able to regulate i_d current to zero. PI-1 presented a much faster speed response, but with greater control peaks and oscillations in the application of loads at 1 s (20 Nm) and 2 s (30 Nm).

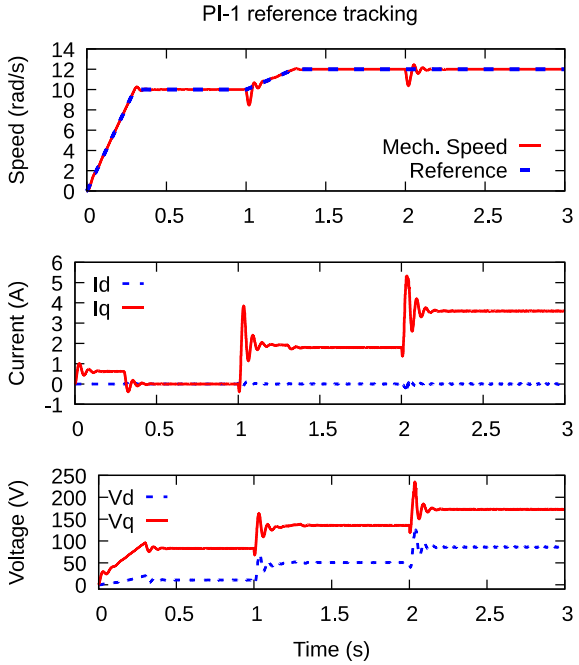

Fig. 2. PI-1 reference tracking with load torque steps.

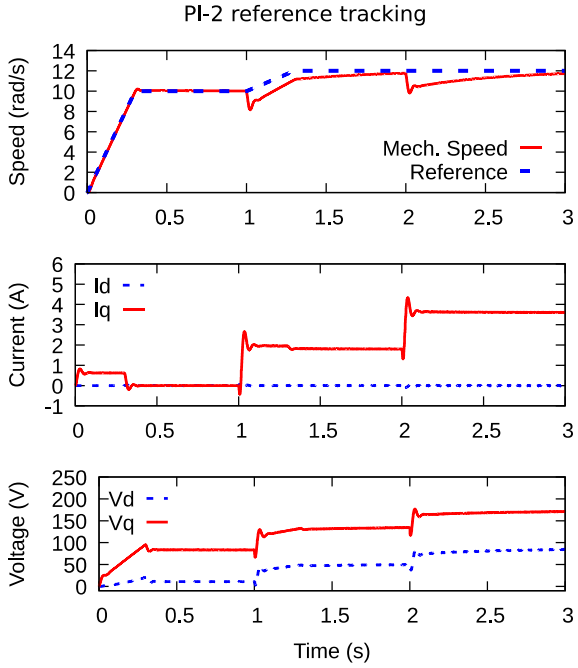

Fig. 3. PI-2 reference tracking with load torque steps.

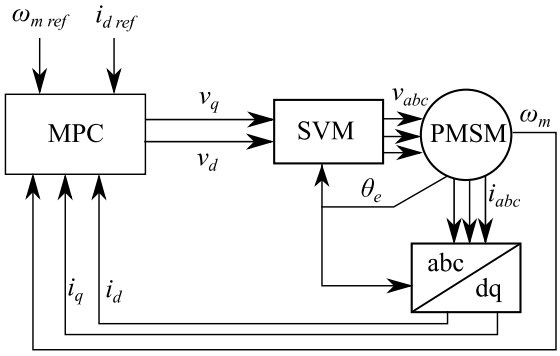

Fig. 4. FOC using multivariable MPC.

IV. MPC CONTROLLER

MPC is a family of digital controllers which operate based on the optimization of the future behavior of the control loop over a given horizon of N samples by using a prediction model [12]. By defining a cost function, an optimization method is used in MPC to find the sequence of M variations in the control actions which minimizes the referred cost function. MPC has the advantages of handling multivariable coupled plants and solving optimization problems with constraints [3].

With a multivariable approach, FOC using MPC is implemented as shown in Figure 4. The controller block receives feedback of ω_m, i_q and i_d. Then, using the prediction model and the references for ω_m and i_d, control actions v_d and v_q are generated through an optimization method. Depending on the employed MPC approach, integrators might be included in the MPC block.

In the following, an overview of the steps to implement the state space MPC strategy is given. For more detailed information, the reader is referred to [3, 13].

In this work, the employed prediction model was obtained from a discrete state space model, obtained by discretization of the continuous state space model in (1). The discretized state space model for the PMSM is given by:

$$x_D(k+1) = A_D x_D(k) + B_D u_D(k) \quad (10)$$

$$y_D(k) = C_D x_D(k) \quad (11)$$

The variables in such model are defined as: $x_D(k) = [i_d(k) \quad i_q(k) \quad \omega_m(k)]^T$, $y_D(k) = [i_d(k) \quad \omega_m(k)]^T$, $u_D(k) = [v_d(k) \quad v_q(k)]^T$, $A_D = I + T_s A_c$ and $B_D = T_s B_c$, where $T_s = 1\ ms$ and A_c and B_c are the continuous state space matrices given in (1).

For including an integrative characteristic to the control loop, the prediction model is augmented to:

$$x(k+1) = Ax(k) + B\Delta u(k) \quad (12)$$

$$y(k) = Cx(k) \tag{13}$$

with

$$A = \begin{bmatrix} A_D & 0 \\ C_D A_D & I \end{bmatrix} \quad B = \begin{bmatrix} B_D \\ C_D B_D \end{bmatrix} \quad C = [0_{2\times3} \quad I_{2\times2}] \tag{14}$$

using $y(k) = [i_d(k) \quad \omega_m(k)]^T$ as output. The state vector is $x(k) = [\Delta i_d(k) \quad \Delta i_q(k) \quad \Delta\omega_m(k) \quad i_d(k) \quad \omega_m(k)]^T$ and the input vector is $\Delta u(k) = [\Delta v_d(k) \quad \Delta v_q(k)]^T$. The operator Δ denotes the variation of a given variable between two sampling periods: $\Delta f(k) = f(k) - f(k-1)$ for a generic variable $f(k)$.

Weighting matrices are defined for the predicted inputs and outputs as Λ and Γ, respectively, by:

$$\Lambda = \begin{bmatrix} \lambda_{\omega_m} & 0 \\ 0 & \lambda_{i_d} \end{bmatrix} \quad \Gamma = \begin{bmatrix} \gamma_{v_d} & 0 \\ 0 & \gamma_{v_q} \end{bmatrix} \tag{15}$$

where λ_{ω_m} and λ_{i_d} are the speed and current predicted errors weights, respectively, and $\gamma_{v_d}$and γ_{v_q} are the input efforts cost weights for v_d and v_q, respectively. Using such weighting matrices, a cost function which consists in a compromise between control efforts and reference tracking can be defined as:

$$\begin{aligned} J_{cost}(k) = &\sum_{j=1}^{N} [y_{error}(k+j|k)]^T \Lambda [y_{error}(k+j|k)] \\ &+ \sum_{j=1}^{M} [\Delta u(k+j-1|k)]^T \Gamma [\Delta u(k+j-1|k)] \end{aligned} \tag{16}$$

in which $f(k+j|k)$ stands for the prediction for variable f at time $k+j$, considering the available information at time k, and $y_{error}(k+j|k) = y(k+j|k) - y_{ref}(k+j)$, where $y_{ref}(k)$ is the output reference. In this work, both $y(k+j|k)$ and $y_{ref}(k+j)$ are 2-dimentional vectors, as there are two outputs in the considered PMSM control system.

It is possible to rewrite the cost function in a vector form, by augmenting the weight matrices to $\bar{\Lambda}$ and $\bar{\Gamma}$ to fit the prediction (N) and control (M) horizons, respectively, as [13]:

$$\bar{\Lambda} = \begin{bmatrix} \Lambda & 0_{2\times2} & \cdots & 0_{2\times2} \\ 0_{2\times2} & \Lambda & \cdots & 0_{2\times2} \\ \vdots & \vdots & \ddots & \vdots \\ 0_{2\times2}0 & 0_{2\times2} & \cdots & \Lambda \end{bmatrix} \tag{17}$$

$$\bar{\Gamma} = \begin{bmatrix} \Gamma & 0_{2\times2} & \cdots & 0_{2\times2} \\ 0_{2\times2} & \Gamma & \cdots & 0_{2\times2} \\ \vdots & \vdots & \ddots & \vdots \\ 0_{2\times2} & 0_{2\times2} & \cdots & \Gamma \end{bmatrix} \tag{18}$$

Also, by using the prediction model for N steps prediction in a vector form, in the unconstrained MPC case, it is possible to obtain an expression for the optimal control increment sequence:

$$\Delta U^* = (H^T \bar{\Lambda} H + \bar{\Gamma})^{-1} H^T \bar{\Lambda} \left[Y_{ref} - \Phi x(k) \right] \tag{19}$$

where

$$H = \begin{bmatrix} CB & 0 & \ldots & 0 \\ CAB & CB & \ldots & 0 \\ \vdots & \vdots & \cdot & \vdots \\ CA^{N-1}B & CA^{N-2}B & \cdots & CA^{N-M2}B \end{bmatrix} \tag{20}$$

and

$$\Phi = [CA \quad CA^2 \quad \ldots \quad CA^N]^T \tag{21}$$

with the N future reference samples contained in Y_{ref}.

Finally, at each sampling instant, ΔU^* is calculated and the first increment of such sequence is applied to the control actions, using the receding horizon strategy [3]. Such strategy is used to allow the controller to update the control actions at each sampling instant, for handling disturbances and errors between the prediction model and the real plant.

The controller parameters were set with $N = 8$, $M = 2$, $\lambda_{\omega_m} = 0.1$, $\lambda_{i_d} = 1$, $\gamma_{v_d} = 0.5/200^2$ and $\gamma_{v_q} = 0.5/200^2$. The horizons were set in a manner that the resulting computational time was at most 0.1 ms (10% of the sampling period) in computer simulation. As the use of a larger control horizon M did not generate significant improvements, the prediction horizon was increased to $N = 8$, with $M = 2$, to achieve the designed computational load. The embedded application can perform a better computational time than the obtained in the simulation [5], which implies a feasible horizon choice. The weighting matrix Λ was set in a manner that speed and current objectives had similar importance, considering that numeric value of the nominal speed is higher than the expected current error values. This was a guided empirical tuning. However, a normalization procedure could also have been done to achieve the same result. The control action weights were set equally, so both speed and current objectives could be fairly considered. A normalizing weight of 200^2 was firstly set, considering a nominal voltage of 200 V, and a coefficient of 0.5 was applied to achieve fast responses without generating higher voltage peaks than the utilized PI controllers.

A test was performed to evaluate the constant reference tracking and load rejection of MPC with SVM. Figure 5 shows the resulting speed, currents and voltages for the MPC controller. Comparing to PI-1, the obtained reference tracking dynamics was similar. The speed oscillations when load torque steps were applied were, however, smaller for MPC, with also lower current and voltage peaks.

V. Frequency Response Results

In this section, the results involving frequency responses are presented. Control saturation was handled with an anti-windup strategy for the PI controllers. The utilized MPC methodology is unconstrained and based on control increments, without integrating errors. Thus, simple saturators were used for MPC. In all simulations, a limit of ±200 V was applied to both input voltages v_d and v_q.

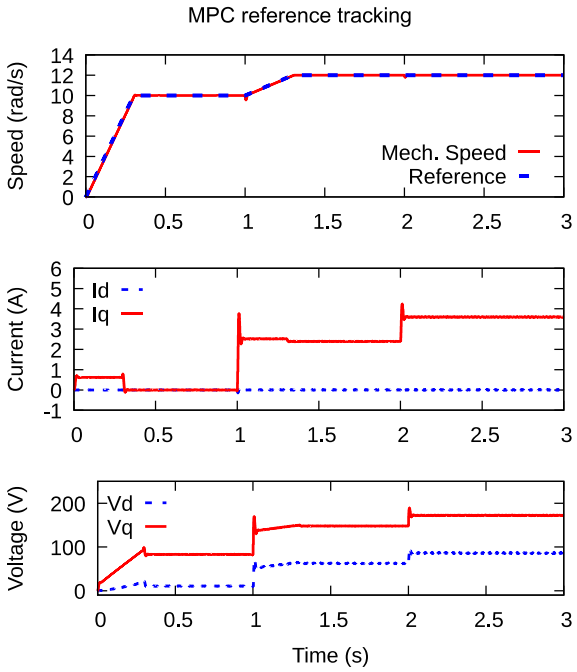

Fig. 5. MPC reference tracking with load torque steps.

A. *Dynamic stiffness*

Dynamic stiffness is defined as the amplitude of a disturbance, in a given frequency, which produces an output response with unitary amplitude in a dynamic system [7]. In the case of an electric motor, it is interesting to observe the effects of a load torque, as a disturbance, and the resulting closed-loop speed oscillation, as the response.

To perform the dynamic stiffness measurement, the controllers PI-1, PI-2 and MPC were tested by varying the frequency of a sinusoidal load torque of amplitude 5 Nm. Such disturbance was applied over an operational speed point of $\hat{\omega}_m$= 10 rad/s and 20 Nm of constant load torque. Figure 6 shows the result of one of the tests performed with PI-I, with a 10 Hz torque disturbance.

The speed output for the same test using MPC is shown in Figure 7. MPC rejected the disturbance with more attenuation than PI-I at 10 Hz, due to its higher speed bandwidth. The objective of such comparison is to show that a cascade free control loop is able to better attenuate low frequency AC disturbances using the same switching frequency than the PI-based cascaded control strategy, which was designed to achieve the highest closed-loop bandwidth while respecting a bandwidth limit due to the switching frequency for the current loop and a decoupling limit for the speed loop. The dynamic stiffness is then calculated as the amplitude of the disturbance divided by the amplitude of the speed response oscillation. Collecting simulation data from 2 Hz up to 200 Hz of disturbance, a dynamic stiffness plot was created, considering the three tested controllers. The resulting plot is shown on Figure 8. It is possible to observe that, at low frequencies, in which the controller is the main responsible for the stiffness, MPC presented the best result, while PI-1 over-performed PI-2. At medium frequencies (from 30 Hz to 100 Hz), the PI controllers presented a slightly greater stiffness than MPC and, as the frequency increases, all controllers result in the same stiffness. This occurs because at high frequencies the controllers do not have enough bandwidth to reject the disturbance, but the motor inertia attenuates the oscillations, which has the same effect for the three control loops.

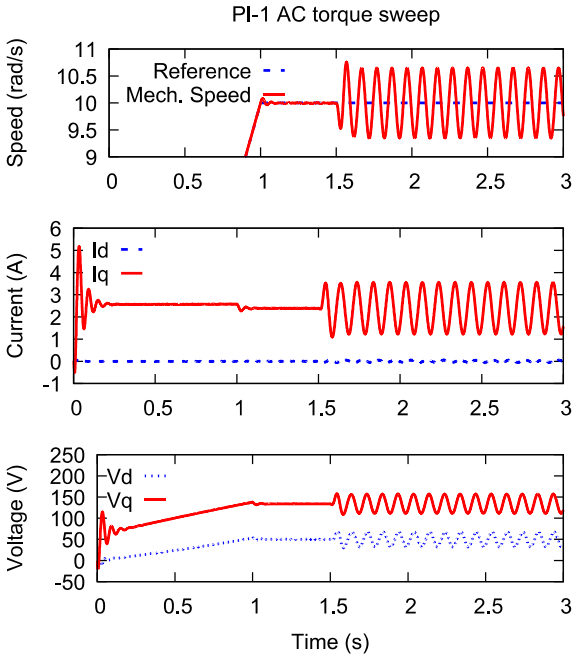

Fig. 6. AC torque sweep procedure with PI-1 at 10 Hz.

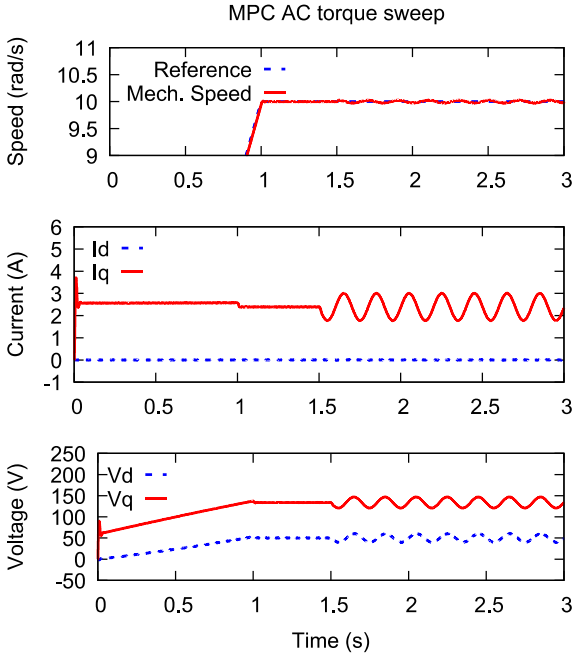

Fig. 7. AC torque sweep procedure with MPC at 10 Hz.

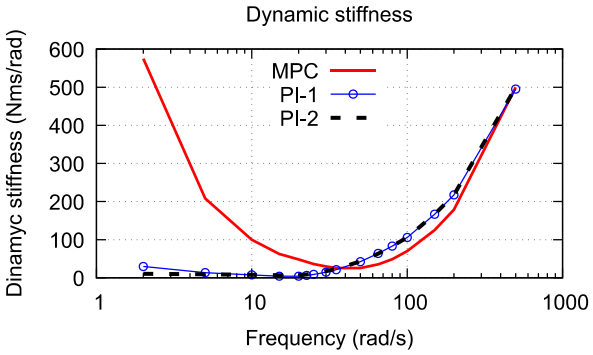

Fig. 8. Dynamic stiffness using MPC and both PIs;

B. *AC reference sweep*

The frequency analysis was also performed using sinusoidal speed reference signals over the same operational point as in the stiffness test. In this analysis, the MPC controller was tested in two conditions. The first, MPC-1 users a vector Y_{ref} with all elements equal to the instant reference. In the second, MPC-2, the future reference within the prediction was informed to the controller. Figure 9 shows an AC reference sweep for MPC-1 at 10Hz, over an operating speed $\hat{\omega}_m$= 5 rad/s, while Figure 10 presents the same procedure for PI-1.

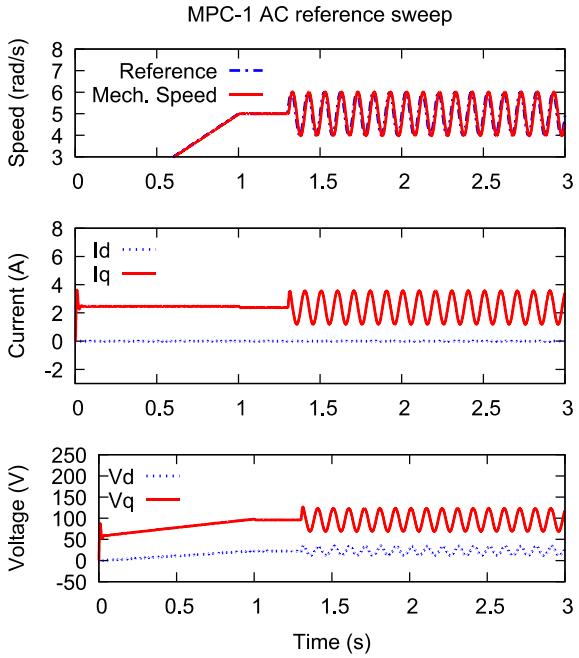

Fig. 9. AC reference sweep procedure with MPC-1 at 15 Hz.

It can be observed that i_d was regulated to zero in both approaches. The obtained speed with MPC-1 presented a practically unitary gain, while with PI-1 the speed was amplified in relation to the reference. Using a higher operating point than $\hat{\omega}_m$= 5 rad/s for the AC reference sweep caused instability problems between 10 Hz and 25 Hz with PI-1 due to control saturation.

The resulting Bode diagram for the four tested controllers, PI-1, PI-2, MPC-1 and MPC-2, is presented in Figures 11 and 12. Firstly, it can be observed that the MPC controllers presented a larger bandwidth than the PIs. Secondly, PI-1 started with a higher gain than PI-2, presenting a maximum value of approximately 7.88 dB. For frequencies higher than 30 Hz, PI-1 and PI-2 presented very similar responses. This means that at such frequencies the proportional gain, that is the same in both PI-1 and PI-2, is the main actuating component.

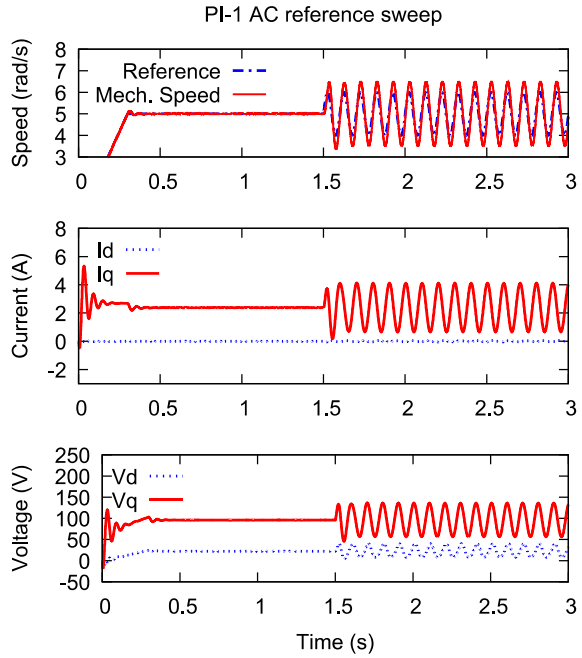

Fig. 10. AC reference sweep procedure with PI-I at 15 Hz.

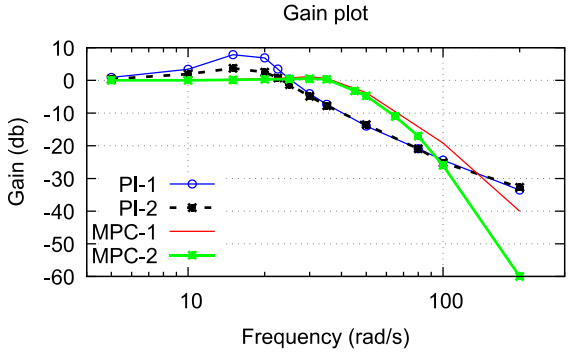

Fig. 11. Gain curves using MPC-1, MPC-2, PI-1 and PI-2.

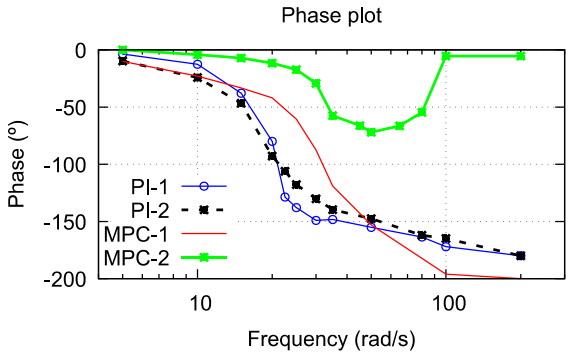

Fig. 12. Phase curves using MPC-1, MPC-2, PI-1 and PI-2.

Observing the phase plot, it is possible to conclude that the reference anticipation resulted in a significantly phase delay reduction for MPC-2, when compared to MPC-1. PI-1 and PI-2 presented similar characteristics, starting at nearly 0, moving towards $-180°$. It is interesting to notice that MPC-2 had a positive slope in phase starting from 50 Hz. However, at higher frequencies, the attenuation of MPC-2 was almost total.

VI. CONCLUSION

In this work, two control approaches were tested for a PMSM SVM-FOC drive with a relatively low switching frequency of 1 kHz. A low frequency modulation enhances the results obtained with MPC, since the PI cascade controllers need to be designed with decoupling frequency margins. The results with the PI controllers, however, are satisfactory, since they are very simple controllers with a smaller computational cost than MPC. The MPC controller, by its turn, presented a more significant stiffness curve for low frequency disturbances and larger bandwidth than the PIs. With a low switching frequency the commutation losses and the cost of inverter compounds are lower, and the MPC can be applied to better explore this condition.

With the present study, the most significant performance improvement by using MPC in relation to PI control is the better disturbance attenuation and trajectory tracking for low frequencies. This is important in a range of applications, since PMSMs are widely used in home appliances, such as washing machines, in which the motor is subject to low frequency mechanical disturbances.

ACKNOWLEDGEMENT

The authors acknowledge Santa Catarina State University for the financial support to G. H. Negri, by means of the Graduate Monitoring Scholarship Program (PROMOP), and Tutorial Learning Program (PET) from the Ministry of Education of Brazil.

REFERENCES

[1] P. Pillay and R. Krishnan, "Modeling, Simulation, and Analysis of Permanent-Magnet Motor Drives, Part I: The Permanent-Magnet Synchronous Motor Drive", *IEEE Transactions on Industry Applications*, vol. *25,* no. 2*,* pp*. 265-273,*March, 1989.

[2] P. Pillay and R. Krishnan, "Modeling of permanent magnet motor drives*", IEEE Transactions on Industry Applications*, vol. *35,* no. 4*,* pp*. 537-541* ,November, 1988.

[3] J. M. Maciejowski. *Predictive Control with Constraints.* Prentice-Hall, Harlow, 2002.

[4] M. Preindl and S. Bolognani, "Comparison of direct and pwm model predictive control for power electronic and drive systems". In *2013 Twenty-Eighth Annual IEEE Applied Power Electronics Conference and Exposition (APEC)*, pages 2526 – 2533, Long Beach, CA, USA, 2013.

[5] M. Preindl and S. Bolognani, "Optimal state reference computation with constrained mtpa criterion for pm motor drives", IEEE Transactions on Power Electronics, vol. 30, no. 8, pp. 4524-4535, 2015.

[6] A. G. Bartsch, G.H. Negri, C. R. Scalabrin, M. S. M. Cavalca, A. Nied and J. de Oliveira, "Predictive control approach for permanent magnet synchronous motor drive", *Eletrônica de Potência*, vol. 20, no. 4, pp. 395–403, 2015.

[7] R. D. Lorenz and P. B. Schmidt, "Synchronized motion control for process automation". In *Conference Record of the 1989 IEEE Industry Applications Society Annual Meeting*, San Diego, 1989.

[8] E. Fuentes, D. Kalise, J. R. and R. M. Kennel, "Cascade-free predictive speed control for electrical drives". *IEEE Transactions on Industrial Electronics*, vol. 61, no. 5, pp. 2176–2184, May 2014.

[9] M. Preindl and S. Bolognani, "Model predictive direct speed control with finite control set of pmsm drive systems". *IEEE Transactions on Power Electronics*, vol. 28, no. 2, pp. 1007–1015, February 2013.

[10] D. W. Novotny and T. A. Lipo. *Vector Control and Dynamics of AC drives*. Oxford Science Publications, 1996.

[11] D. E. Rivera. *Internal model control: A comprehensive view.* Arizona State University, 1999.

[12] S. J. Qin and T. A. Badgwell, "A survey of industrial model predictive control technology", *Control Engineering Practice*, vol. 11, pp. 733–764, 2003.

[13] G. H. Negri, A. G. Bartsch, M. S. M. Cavalca, J. de Oliveira, A. Nied, and A. S. Silveira, "Model-based predictive direct speed control applied to a permanent magnet synchronous motor with trapezoidal back-emf". In *2014 11th IEEE/IAS International Conference on Industry Applications (INDUSCON)*, Juiz de Fora, BR, 2014.

Received: 30 May 2017;
Accepted: 26 January 2018;
Published: 06 April 2018